

# Systematic resistivity study of the pseudogap and critical temperature for (Hg,Re)-1223 superconductors

C. A. C. Passos<sup>1</sup>, M. T. D. Orlando<sup>1</sup>, J. L. Passamai Jr<sup>1</sup>, E. V. de Melo<sup>2</sup>

<sup>1</sup>Departamento de Física, Universidade Federal do Espírito Santo, Vitória - ES, 29060-900, Brazil

<sup>2</sup>Departamento de Física, Universidade Federal Fluminense, Niterói - RJ, 24210-340, Brazil

e-mail: cpassos@coer.ufes.br or capassos@yahoo.com

May 24, 2019

## Abstract

After a detailed characterization of the (Hg,Re)-1223 polycrystalline samples, the pseudogap temperature  $T_{\text{p}}$ , fluctuation temperature  $T_{\text{scf}}$  and the superconducting critical temperature  $T_{\text{c}}$  have been systematically studied through electrical resistivity measurements by several different current densities. Performing many sets of measurements with different current densities we show that, while low current values are desirable because they are in the linear regime, they are plagued by high noise and, on the other hand, high current values are more stable but they yield non-linear terms. Therefore, we have studied the resistivity ( $\rho$ ) by a large interval of current densities in order to obtain an ideal current for each sample. The appropriate current value allows to determine  $T_{\text{p}}$ ,  $T_{\text{scf}}$  and the critical temperature  $T_{\text{c}}$  for three different oxygen content. This method, developed in detail here, and used to derive the (Hg,Re)-1223 phase diagram can be applied to any high critical temperature superconductor (HTSC).

# 1 Introduction

One of the greatest puzzles of the condensed matter physics is to understand the superconducting fundamental interactions of the high  $T_c$  superconductors (HTSC) and their many unconventional properties. Among these, the pseudogap region below  $T_c$  and above  $T_c$  (the so-called pseudogap phase) [1] has attracted a lot of attention in order to determine the precise values of  $T_c$  as function of the doping level  $n$  and, above all, to understand its relation to the superconducting phase. Therefore a large number of different techniques have been used to study the dependence of  $T_c$  for many family of compounds [1, 2].

As discussed in ref. [1] and [2] and in many others [3, 4, 5, 6, 7] an important tool to study  $T_c(n)$  is the transport properties by electrical resistivity measurements. At high temperatures the resistivity ( $\rho$ ) is linear with the temperature and  $T_c(n)$  is defined as the temperature which  $\rho(T)$  decreases below the linear behavior. However, it is well known that there are considerable differences in the values of  $T_c(n)$  found in the literature. We attempt here to define a systematic approach to this problem.

There are many parameters which can determine with accuracy the resistance measurements above the  $T_c$ . As considering polycrystalline samples, these factors are: the type of morphology, junctions, the cross section size of the grains and stoichiometry in the grain [8]. However, the most important factor is the applied current density value and its influence on the resistivity measurements done in polycrystal or single crystal. Therefore, it is an open question about the precision of the resistance measurements, that means: what would be the ideal current applied to the polycrystalline sample? A quickly search in the literature shows that there is no consensus about what is the ideal current which must be used at the four-point probe. For instance, in the case of thin films, Qiu et al. [9] have applied a current of 0.01 mA ( $J = 1.5$  A/cm<sup>2</sup>), and Wuyts et al. [6] have measured the temperature dependences of the resistivity with a current density  $J = 10^2$  A/cm<sup>2</sup>. For polycrystalline samples, Tristan Jover et al. [10] have used a current of 1.8 mA and Batista-Leyva et al. [11] used 0.35 mA. Gonzalez et al. [12] have measured the resistivity within the linear response regime with a current density of 0.07 A/cm<sup>2</sup> applied to the  $\text{Hg}_{0.82}\text{Re}_{0.18}\text{Ba}_2\text{Ca}_2\text{Cu}_3\text{O}_{8+d}$  sample or  $(\text{HgRe})-1223$  sample. In

addition, Palstra et al. [13] have checked the linearity of the I-V curves for currents between 0.1 and 100 mA in single crystals. In this ref. [13], they have found that deviations from linearity start above 30 mA. Therefore, they have chosen a measuring current well below this value at 10 mA ( $J' = 4.5 \times 10^3 \text{ A/cm}^2$ ). As a consequence, although  $T_c$  is very robust to these kind of current variations, it can occur an apparent discrepancy to determine pseudogap temperature  $T^*$ . According to Tallon et al. [2], when the resistivity measurement is plotted to 300 K,  $T^*$  is equal to 195 K, which is defined as the temperature which  $\rho(T)$  goes under the linear regime as the temperature goes down. When, however, the same resistivity data are plotted up to 600 K, a visual inspection yields  $T^*$  at 320 K.

The figure 1 displays a typical resistivity curve as a function of the temperature for a  $\text{Hg}_{0.82}\text{Re}_{0.18}\text{Ba}_2\text{Ca}_2\text{Cu}_3\text{O}_{8+\delta}$  ceram ic produced in our laboratory. As one can see in this figure, the visual inspection may not make a good judgement between pseudogap open and normal state because it depends strongly where one takes the linear regime and the value of the current density. Therefore, the visual criteria does not have the necessary precision to study the  $T^*$  phase diagram.

In this paper we perform a systematic resistivity measurements on three  $(\text{Hg,Re})-1223$  superconductors to determine  $T^*$  as a function of doping carrier number  $n$ , but, in doing these measurements, we outlined a method which the values of  $V = V(I)$  and  $\rho(T)$  are analysed with several values of current  $I$  and temperature  $T$ , in order to find a range of current density which is ideal to determine  $T^*$ . For our surprising and, so far as we know, there is not any published systematic analysis of this type, although this is an important topic.

## 2 Experimental details

### 2.1 Precursor preparation

Firstly, preparation of the ceram ic precursor typical began with a mixture of  $\text{Ba}_2\text{Ca}_2\text{Cu}_3\text{O}_x$  (99.0% PRAXA IR) and  $\text{ReO}_2$  (99.0% Aldrich) in powder form with the molar relationship 1 : 0.18 [14]. These powders were homogenised in an agate mortar and pelletised with an applied

uniaxial pressure of 0.5 GPa. The produced pellet was heated at 850 °C in a flow of oxygen (99.5% purity) for 15 h. The obtained precursor was crushed, homogenised and compacted again before being heated a second time at 920 °C for 12 h in a flow of oxygen. The later procedure is repeated for seven more times. These thermal treatment processes are meant to provide a good homogenisation of the rhenium atoms and to eliminate the carbonates remaining in the precursor sample as it was discussed in more detail previously [15].

## 2.2 Precursor characterization before annealing

It is known that the oxygen stoichiometry may be modified and controlled through the thermal treatment [14, 15, 16]. Regarding this, x-ray powder diffraction pattern (XRD) analysis of each precursor preparation step was done in order to evaluate the oxygen content of the ceramic precursor, as shown in Figure 2. The XRD measurements was carried out with a Rigaku model 4053A 3 with  $\lambda = 1.5418 \text{ \AA}$  and CuK  $\alpha$  radiation. The identified phases were  $\text{BaCuO}_{2+x}$  (101 phase),  $\text{Ba}_2\text{Cu}_3\text{O}_{5+x}$  (203 phase),  $\text{Ba}_4\text{CaCu}_3\text{O}_{8+x}$  (413 phase),  $\text{Ca}_2\text{CuO}_3$  and  $\text{Ca}_5\text{Re}_2\text{O}_{12}$ . The x-ray spectra show a change in the relative reflection intensity, which is represented by the line above the peaks. It can be seen that there is a variation in the effective integrated area of the peaks  $2\theta = 30.07^\circ$  and  $2\theta = 30.72^\circ$ . The phases  $\text{BaCuO}_{2+x}$  and  $\text{Ca}_5\text{Re}_2\text{O}_{12}$  are associated with  $2\theta = 30.07^\circ$ , and the phases  $\text{Ba}_2\text{Cu}_3\text{O}_{5+x}$  and  $\text{Ba}_4\text{CaCu}_3\text{O}_{8+x}$  are associated with  $2\theta = 30.72^\circ$ . The increase of the 413 phase minimizes the formation of  $\text{HgCaO}_2$  impurity [17], and as a consequence, this favors the superconductor synthesis. This change of behavior in the peaks has also been observed by Sin et al. [14] in precursor samples, where different thermal treatments were applied.

## 2.3 Precursor annealing

The obtained precursor material was then submitted to an annealing at 920 °C for 24 h in a flowing of gas mixture of argon (99.5% purity) and oxygen (99.5% purity) maintained at 1 bar. Three ceramic precursors were prepared with distinct partial pressure of oxygen: 5% of  $\text{O}_2$  and

95% of Ar (sample A), 10% of O<sub>2</sub> and 90% of Ar (sample B) and 15% of O<sub>2</sub> and 85% of Ar (sample C) [18]. In order to control the oxygen content and the argon gas mixture, a Quanta Chrom e Inc. gas mixer, with controlled flow rate, was used [16].

The influence of oxygen partial pressure over each precursor was analysed by x-ray diffraction measurements with  $\lambda = 1.5418 \text{ \AA}$  and CuK  $\alpha$  radiation. These measurements were done in the Laboratory National of Light Synchrotron - Campinas, Brazil and are shown in figure 3. The identified phases also were BaCuO<sub>2+x</sub> (101 phase), Ba<sub>2</sub>Cu<sub>3</sub>O<sub>5+x</sub> (203 phase), Ba<sub>4</sub>Cu<sub>3</sub>O<sub>8+x</sub> (413 phase), Ca<sub>2</sub>CuO<sub>3</sub> and Ca<sub>5</sub>Re<sub>2</sub>O<sub>12</sub>. It could be noted that the peaks associated with 101 phase, which has oxygen stoichiometry variation, are slightly displaced to low angles. This is an indication that there was an oxygen increment of the precursors ceramics B and C, as compared with ceramic A. It is important to state that these peak displacements are not zero shift of diffraction center, because the Ca<sub>2</sub>CuO<sub>3</sub> peaks have not presented this same displace, as it is shown in figure 3.

## 2.4 Superconductor synthesis

Finally, the precursors prepared with different O<sub>2</sub> partial pressure were blended with HgO at molar relationship 1 : 0.82. They were also homogenised in an agate mortar and pelletised with an uniaxial pressure of 1 GPa. The pellets with a typical dimensions 5 × 5 × 20 mm<sup>3</sup> were wrapped in a gold foil (99.999%) and introduced in a quartz tube with 8 mm inner diameter. Furthermore, it was introduced together with each pellet a rod of quartz (7 mm diameter and 40 mm length). Each sample (A, B and C) wrapped with a gold foil has received an excess of Hg (l) in amalgam form. The ratio between the mercury mass and the gold mass was 0.045. Basing on the study of the quartz tube filling factor effect ( ) [19], it was used  $\rho = 1.0 \text{ g.cm}^{-3}$  and  $\rho_{\text{Hg}} = 0.010 \text{ g.cm}^{-3}$  [16]. The quartz tubes were sealed in a high vacuum of  $3 \times 10^{-6}$  torr. All procedures were taken place inside a glove box filled with argon gas. In order to improve the grain size growing, the annealing time have changed to 72 h at 865 °C, as compared to Sine et al. [18]. Moreover, three sealed quartz tubes, each one with a sample inside, were installed together in the same place inside an isostatic pressure furnace. The furnace was filled with 14

bar of Ar in order to avoid an explosion of any quartz tube.

## 2.5 Superconductor characterization

The samples with different partial pressure of oxygen were also analysed by XRD patterns, and the result is displayed in figure 4. For all samples, the (Hg,Re)-1223 phase was the main phase present (96%), and slight impurities were detected [8]. In addition, the overdoped sample presented a trace of the HgCaO<sub>2</sub> composition, which is in accordance to Sin et al. [17].

The superconductor samples A, B and C were submitted to ac magnetic susceptibility which have yielded  $T_c$  (132.6, 133.2 and 132.7 K). The results suggest that the samples have similar oxygen contents which are in agreement with the ref. [14]. A small difference in  $T_c$  is explained taking into account the fact that rhenium is the main oxygen doping mechanism in these materials, providing extra oxygen atoms in the HgO layers [20]. For the Hg-1223 (without rhenium), the oxygen found at the (1/2,1/2,0) are responsible for the doping variation since they are loosely bond to the Hg atoms. This mechanism leads to easy intercalation or removal of the oxygen during the synthesis. However, in the (Hg,Re)-1223 sample, there is the covalent Re-O bond which has presented an oxygen at (0.33, 0.33,0) where the bond must be stronger. Therefore, the Re-O bond present in 20% of the sample would be unlike the HgO layers oxygens and it may not be removed with a lower oxygen partial pressure present in the synthesis process.

Sin et al. [14] have shown the phase diagram of (Hg,Re)-1223 as a function of the oxygen partial pressure ( $P_{O_2}$ ) of the precursor. For precursor prepared with  $P_{O_2} = 0.2$  bar, it was found a single (Hg,Re)-1223 phase and a slightly  $T_c$  parabolic variation.

It was shown in our previous paper [8] that the  $T_c$  value is not enough parameter to define the oxygen contents in (Hg,Re)-1223 system. It was observed that the ac susceptibility measurements under external hydrostatic pressure is an important tool to confirm the difference of oxygen contents. These samples have presented distinct  $dT_c/dP$  values 8.1, 1.9.2 and -1.6.1 K GPa<sup>-1</sup>, which confirm the underdoped, optimally doped and overdoped oxygen contents, respectively. In order to confirm this, thermopower measurements were done on present sample

set..

## 2.6 Therm opower m easurem ents

The therm opower was measured on pellets of size  $1 \times 1 \times 7 \text{ mm}^3$ . Each pellet was mounted with a small resistance heater on the top and fixed on a sapphire sample holder at its bottom. The therm opower measurements were carried out at constant temperature controlled by a Lake Shore Temperature 330 controller. Temperature gradients  $\approx T_x$  the order of  $0.5 \text{ K/mm}$  were applied using a KEITHLEY 228A power source to supply a controlled power on the small resistance heater. The  $T_x$  were measured by a calibrated Au/0.07 at% Fe-Chrom el-P thermocouples made by Leico Industries Inc., and using a HP 34401A digital multimeter. The voltage between the top and bottom of each sample was measured by a KEITHLEY 182 nanovoltmeter. All instruments were controlled and read by a IEEE-488 GPIB communication setup [21].

The results are shown in the figure 5, and it can be noted that the therm opower signals  $S$  have a typical behavior described by MacIntosh and Kaiser [22]. Moreover, the therm opower signal is positive and distinct at room temperature. The high- $T_c$  superconductor cuprates have been found to show a parabolic variation of  $T_c$  as a function of hole concentration function,  $T_c = T_c^{\text{max}} - 82.6T_c^{\text{max}}(n - 0.16)^2$  [2, 23]. Oberelli et al. [24] proposed a universal dependence of the thermoelectric power signal ( $T = 290 \text{ K}$ ) on the hole concentration. In general, close to  $n = 0.20$  the thermoelectric power changes the sign from positive to negative.

For the HgBa<sub>2</sub>Cu<sub>2</sub>O<sub>8+</sub> [25] compounds, the hole concentration was found to be  $n = 0.20$ , which maintains a positive thermoelectric power signal up to room temperature. The results are summarized in table 1. The number of holes  $p$  were determined by the Oberelli et al. [24] universal behavior.

The (Hg,Re)-1223 compounds have a hole concentration  $n < 0.20$ . This fact is justified by the phase diagram proposed by Sin et al. [14]. When a  $P_{\text{O}_2} > 0.2$  bar is used in the precursor annealing (overdoped), the (Hg,Re)-1223 material exhibits a segregation of (Hg,Re)-1212 and HgCuO<sub>2</sub> phases. As demonstrated by the thermobarometric analyser (TBA) *in situ* measurement [19], the oxygen pressure increases atmosphere in the sealed quartz tube at the synthesis

process. The increase of partial pressure of oxygen, inside the quartz sealed tube, shifts the equilibrium in order to favor the  $(\text{HgRe})-1223$ ,  $(\text{HgRe})-1212$  and  $\text{HgCaO}_2$  phases. Since the  $(\text{HgRe})-1212$  and  $\text{HgCaO}_2$  phases are rich in the oxygen, these phases provoke a reduction of the oxygen content present in the  $(\text{HgRe})-1223$ . This is the reason why negative thermoelectric power signal is not found in  $(\text{HgRe})-1223$  system, when the oxygen partial pressure  $P_{\text{O}_2}$  is increased above 0.20 bar.

## 2.7 SEM and EDS analysis

As described before [8], the oxygen partial pressure inside the sealed quartz tube was influenced by the precursor annealing. For the phase diagram region  $P_{\text{O}_2} < 0.2$  bar, the effect of the  $P_{\text{O}_2}$  pressure on the junction crystal size was not analysed until now. With this aim in mind, we have obtained Scanning Electron Microscopy (SEM) images and an Energy Dispersive X-ray Spectra (EDS) analysis of the samples (see table 2) [8], which also indicates the stoichiometry of the  $\text{Hg, Re, Ba, Ca, and Cu}$  elements present in the three samples. Using the SEM images [8] of sample B (see figure 6), a histogram of the grain-boundary size was done. This procedure was also done for sample A and sample C [8]. From these SEM images, the average junction sizes  $\langle d \rangle$  were determined and are shown in table 2.

Summarizing, the samples have similar morphology of the grains, average junction sizes are also similar and same type junction (superconductor – insulate – superconductor), as reported elsewhere [26].

## 2.8 Resistivity setup measurements

The dc electrical resistance of the samples was measured using the four-point probe method. The samples were cut in slab form with dimensions of  $1.2 \times 1.0 \times 7.0 \text{ mm}^3$  and they were fixed on a sapphire sample holder by using GE varnish. The four contacts with low electric resistance ( $5 \Omega$ ) were attached to the samples with silver paint. A KEITHLEY 228A Current Source applied currents from  $0.4 \text{ mA}$  up to  $10 \text{ mA}$  at a fixed temperature, and the corresponding voltage values were obtained using a KEITHLEY 182 sensitive digital voltmeter.

The I-V curves were measured reversing the current direction during measurement in order to avoid contact resistance influence. The temperature was measured by a copper-constantan thermocouple attached to the sapphire and linked to the HP 34401A multimeter. All data were recorded by a PC computer by IEEE-488 interface.

### 3 Electrical resistivity analysis

#### 3.1 Pseudogap temperature

In general, the dependence of average voltage on the current can be written as the following expansion

$$V = R_1 I + R_2 I^2 + \dots; \quad (1)$$

where  $R_1 = R_1(T)$  and  $R_2 = R_2(T)$ .

In figure 7 we plot the curves  $V = V(I)$  for only one of our samples since the curves for the others have the same features. The curve at 170 K represents the temperature where one expects to find  $T_c$ . This figure shows that  $V = V(I)$  is a linear function up to  $J = 4 \text{ A/cm}^2$ . However, for lower temperatures,  $T$  close to  $T_c$ , non-linear effects develop in the  $V(I)$  due to a non-vanishing value of  $R_2$ . As the figure 7 shows, for  $T = 145 \text{ K}$  we have found that non-linear behavior appears above  $J > 1.04 \text{ A/cm}^2$ . Thus, in order to obtain the high temperature linear behavior and the value of  $T_c$  accurately, one has to use  $J = 1 \text{ A/cm}^2$  for sample B. Accordingly, the same analysis for sample A yields the maximum linear current  $J = 1.05 \text{ A/cm}^2$  and sample C,  $J = 1.00 \text{ A/cm}^2$ . Thus, in what follows, we will make the analysis with  $J = 1.00 \text{ A/cm}^2$  for all the samples measured in this work.

Taken into account the current values above, which assure us that the systems are in the linear regime ( $R_2 = 0$ ), we can write that

$$R_1(T) = R_0 + \frac{\partial R}{\partial T}(T - T_0) + \frac{\partial^2 R}{\partial T^2}(T - T_0)^2 + \dots; \quad (2)$$

what shows that the resistivity is linear with the temperature, whenever  $\partial^2 R / \partial T^2 = 0$  and  $\partial R / \partial T$  is independent of the temperature. This behavior is found for most HTSC at  $T > T_c$ .

From the electrical resistivity study, we can determine the values of  $T_c$  (n) analysing the first ( $\frac{d}{dT} = \frac{dT}{d\Omega}$ ) and second ( $\frac{d^2}{dT^2} = \frac{dT^2}{d\Omega^2}$ ) derivatives of the resistivity with respect to the temperature. The study of the second derivative has been used recently by Ando et al. [27] to study the pseudogap phase of many compounds. Furthermore, Naqib et al. [28] have estimated  $T_c$  above and below  $T_c$  and also the superconducting fluctuation temperature  $T_{scf}$  using the same method. They verified that for nearly identical values of number of holes, both sintered and high oriented thin film of  $Y_{1-x}Ca_xBa_2(Cu_{1-y}Zn_y)_3O_7$  have the same values for  $T_c$ . The only difference between polycrystalline sample and thin film is the residual resistivity value. The polycrystal has a residual resistivity value much larger due to percolative effect and great contributions from the grain boundaries.

As mentioned here, the resistivity must be analysed at low density of current to avoid the non-linear regime. On the other hand, lower values of  $J$  are susceptible to high resistivity oscillations and does not allow an accurate estimation on  $T_c$ . Figures 8a, 8b, 8c shows  $(\frac{d}{dT} = \frac{dT}{d\Omega}) = (\frac{d}{dT})_{T=170K}$  and  $\frac{d^2}{dT^2} = \frac{dT^2}{d\Omega^2}$  for  $J = 1 \text{ A/cm}^2$ . Thus, after study of the non-linear effects, we have chosen values of  $J = 1 \text{ A/cm}^2$  as a linearity limit for our three samples. In these curves one can see that  $(\frac{d}{dT} = \frac{dT}{d\Omega}) = (\frac{d}{dT})_{T=170K}$  increases as the temperature is reduced down to  $T_c$ , however all samples have presented a constant value near 170 K. Consequently the  $\frac{d^2}{dT^2} = \frac{dT^2}{d\Omega^2}$  term is zero for  $T = 170 \text{ K}$  characterizing the high temperature regime, as discussed in the electrical resistivity analysis.

The results plotted in figure 8a, 8b and 8c yield  $T_c = (160 \pm 2) \text{ K}$  for sample A,  $T_c = (154 \pm 2) \text{ K}$  for sample B and  $T_c = (151 \pm 2) \text{ K}$  for sample C. The uncertainties were estimated taking into account the interval where the  $(\frac{d}{dT} = \frac{dT}{d\Omega}) = (\frac{d}{dT})_{T=170K}$  curves start to display a deviation from the background and in the range of temperature which  $\frac{d^2}{dT^2} = \frac{dT^2}{d\Omega^2}$  is vanish.

### 3.2 Fluctuation temperature

The high- $T_c$  superconductors exhibit complex behavior which is related to thermodynamic fluctuations of the superconducting order parameter. These fluctuations affect the electric

cal resistivity characteristics in both normal and superconducting states. The thermodynamic fluctuations near the transition was first studied by Ginzburg [29]. These effects in type I superconductor were shown negligible, after that Aslamasov and Larkin [30] have considered effects of fluctuating pairs of electrons at the conductivity in a metal. Besides Lawrence and Doniach (LD) [31] have proposed a theory of layer structure superconductors where it occurs a crossover of the dimensionality of the fluctuation at a temperature  $T_{scf}$ . They have admitted that a layer was coupled to adjacent 1+1 and 1-1 by Josephson tunneling. Hg<sub>0.82</sub>R<sub>0.18</sub>Ba<sub>2</sub>Ca<sub>2</sub>Cu<sub>3</sub>O<sub>8+δ</sub> compound has presented more complex structure of layers, because there are two different types of CuO<sub>2</sub> layers: inner and outer [32].

The excess conductivity above  $T_c$  was calculated by Aslamasov and Larkin (AL) [30] using a microscopic approach in the mean field region and they obtained a power law [5]

$$(\Delta T) = C \quad (3)$$

with  $\Delta T = (T - T_c)/T_c$

$$C = \frac{e^2}{16\pi d}; \quad = 1 \quad \text{for 2D} \quad (4)$$

$$C = \frac{e^2}{32\pi z}; \quad = \frac{1}{2} \quad \text{for 3D}. \quad (5)$$

Here  $\Delta T$  is the critical exponent related to the dimension of the fluctuations,  $z$  is the coherence length in the z-direction for 3D fluctuations and  $d$  is characteristic thickness for 2D system. In order to verify the different nature between  $T_c$  and thermodynamic fluctuations temperature ( $T_{scf}$ ), we performed an investigation about the fluctuation conductivity  $\sigma_{scf}$  using  $J = 1 \text{ A/cm}^2$ . In this work it was assumed that the outer CuO<sub>2</sub> layers play the role of the layers in the Lawrence and Doniach (LD) theory. The inner CuO<sub>2</sub> layer only coupling the outer CuO<sub>2</sub> layers. Thus, we can use LD approach in order to obtain the interlayer coupling energy  $U_c$ . It was fitted for three samples the linear  $T$ -dependent resistivity  $\rho_n = a + bT$  in the interval 220-270K. For all cases, the fluctuation conductivity  $\sigma_{scf}$  was obtained by subtracting the measured conductivity  $1/\rho_n(T)$  from the normal state conductivity  $1/\rho_n(T)$  [33]:

$$\sigma_{scf} = \frac{1}{\rho_n(T)} - \frac{1}{\rho_n(T)} \quad (6)$$

In figure 9 it shows the dependence of  $\ln T_{\text{scf}} = \ln (T_c)$  with the  $\ln (T - T_c) = T_c$  for sample B. Moreover, one can see the crossover between the slope of -1 to  $-1/2$ , which is so-called Lawrence-Donach temperature [31]:

$$T_{\text{scf}} = T_c [1 + \frac{m}{M} (\frac{2}{s})^2] \quad (7)$$

$$T_{\text{scf}} = T_c (1 + \frac{2}{s}) \quad (8)$$

and

$$\frac{2}{s} = \frac{m}{M} (\frac{2}{s})^2 \quad (9)$$

$$\frac{2}{s} = (\frac{2}{z})^2; \quad (10)$$

where  $z$  is the coherence length in the  $z$ -direction and  $s$  is the layers spacing. On the other hand, if we multiply the equation 7 by the Boltzmann constant  $k_B$  [33], we have:

$$\frac{2}{s} = \frac{U_c}{k_B T_c} \quad (11)$$

where  $U_c$  is the interlayer coupling energy, inversely proportional to the square of interlayer distance. A summary of the results are displayed in table 3.

The change of slope showed in figure 9 indicates a crossover from two-dimensional (2D) to three-dimensional (3D) behavior. It can also note the crossover temperature  $T_{\text{scf}}$  is sensible to oxygen content (table 3). It is important to note that  $T_{\text{scf}}$  presented a different nature as comparing with  $T_c$ , according to the proposed by Naqib et al. [28]. Our measurements have confirmed the 2D character of the fluctuation spectrum, which is expected down to  $(T_{\text{scf}} - T_c) = T_c = 0.01$  (see table 3) for (Hg,Re)-1223 system [34].

## 4 Conclusion

In this paper we have presented the  $T_c(n)$  and  $T_{\text{scf}}(n)$  phase diagram (figure 10) for the three compounds of the (Hg,Re)-1223 family calculated by standards resistivity data. A comparison

ing with others works, our calculations were made only after a very careful analysis of the voltage-current ( $V(I)$ ) isotherms in order to investigate the best range of current density and temperature where  $V(I)$  is in the linear regime. We determined the appropriate range of current to study  $T_c(n)$  for all three samples which are similar in structure and different only by a few percents of oxygen. Our conclusion is that a current value  $J' = 1 \text{ A/cm}^2$  represents the linearity limit for our samples. As considering  $T_c(n)$  defined by the beginning of magnetic measurements [8], the values of  $T_c(n)$  and the oxygen content evaluated by thermopower measurements (see section 2.6), we draw the  $T_c(n)$  and  $T_c(n)$  curves. In figure 10, our values of  $T_c(n)$  above  $T_c(n)$  agree with the general trends found by Naqib et al. [28] that  $T_c(n)$  is above  $T_c(n)$  near the optimum value and should merge into  $T_c(n)$  for  $n = 0.17 - 0.18$ . On the other hand, our results indicate that  $T_c(n)$  merge to  $T_c(n)$  only in the far overdoped regions. We have also determined  $T_{scf}$  which is clearly distinct of  $T_c(n)$  (see table 3). Naqib et al. also were able to distinguish between  $T_c(n)$  and  $T_{scf}$  when resistivity measurements are done under applied magnetic field. They compared the results of polycrystalline, thin film and single crystal cuprate superconductors and found that  $T_c(n)$  is independent of crystalline state of samples [35]. Our conclusion is that any resistivity study of the  $T_c(n)$ , for a given compound, needs to include the investigation about what is an optimal current used for each sample because, the general procedure described here avoids any influence of the non-linear terms produced by the selection of high current density values.

## 5 Acknowledgments

We would like to thank CNPq Grant CT-Energ 504578/2004-9, CNPq-FAPERJ Process E 26/171168/2003 and CAPES for financial supports. Thanks also to the Companhia Vale do Rio Doce (CVRD), Companhia Siderurgica de Tubarão (CST). We gratefully acknowledge to National Laboratory of Light Synchrotron - LNLS, Brazil (# XDR 1/2371)

## References

- [1] T. T. Imusk and B. Statt, *Rep. Prog. Phys.* 62 (1999) 61.
- [2] J. L. Tallon and J. W. Loram, *Physica C* 349 (2001) 53.
- [3] A. Fukuoka, A. Tokiwa Yamamoto, M. Itoh, R. Usami, S. Adachi, and K. Tanabe, *Phys. Rev. B* 55 (1997) 6612.
- [4] E. V. de Melo, M. T. D. Orlando, J. L. González, E. S. Caixeiro, and E. Baggio-Saitovich, *Phys. Rev. B* 66 (2002) 092504.
- [5] Q. Wang, G. A. Saunders, H. J. Liu, M. S. Acres and D. P. A. Mond, *Phys. Rev. B* 55 (1997) 8529.
- [6] B. Wuyts, V. V. Moshchalkov and Y. Bruynseraede, *Phys. Rev. B* 53 (1996) 9418.
- [7] L. J. Shen, C. C. Lam, J. Q. Li, J. Feng, Y. S. Chen and H. M. Shao, *Supercond. Sci. Technol.* 11 (1998) 1277.
- [8] C. A. C. Passos, M. T. D. Orlando, F. D. C. Oliveira, P. C. M. da Cruz, J. L. Passamai Jr, C. G. P. Orlando, N. A. Eloi, H. P. S. Corrêa and L. G. M. Martínez, *Supercond. Sci. Technol.* 15 (2002) 1177.
- [9] X. G. Qiu, B. Wuyts, M. Maenhoudt, V. V. Moshchalkov, and Y. Bruynseraede, *Phys. Rev. B* 52 (1995) 559.
- [10] D. Tristan Jover, R. J. Wijngaarden, R. Griessen, E. M. Haines, J. L. Tallon and R. S. Liu, *Phys. Rev. B* 54 (1996) 10175.
- [11] A. Batista-Leyva, R. Cobas, M. T. D. Orlando, C. Noda, E. A. Ithuler, *Physica C* 314 (1999) 73.
- [12] J. L. González, E. S. Yague, E. Baggio-Saitovitch, M. T. D. Orlando and E. V. L. de Melo, *Phys. Rev. B* 63 (2001) 54516.

[13] T . T . M . Palstra, B . Batlogg, L . F . Schneemeyer, and J . V . W aszczak, *Phys. Rev. Lett.* 61 (1988) 1662.

[14] A . Sin, A . G . Cunha, A . Calleja, M . T . D . O rlando, F . G . E m m erich, E . Baggio-Saitovitch, M . Segarra, S . Pioland X . Obradors, *Supercond. Sci. Technol.* 12 (1999) 120.

[15] S . M . Loureiro, C . Stott, L . Philip, M . F . Gorius, M . Perroux, S . Le Floc'h, J . J . Capponi, D . Xenikos, P . Toulemonde and J . L . Tholence, *Physica C*, 272 (1996) 94.

[16] M . T . D . O rlando, A . G . Cunha, S . L . Bud'ko, A . Sin, L . G . M artinez, W . Vanoni, H . Belich, X . Obradors, F . G . E m m erich and E . Baggio-Saitovitch , *Supercond. Sci. Technol.*, 13 (2000) 140.

[17] A . Sin, A . G . Cunha, A . Calleja, M . T . D . O rlando, F . G . E m m erich, E . Baggio-Saitovitch, S . Pinol, J . M . Chimenos and X . Obradors, *Physica C*, vol. 306 (1998) 34.

[18] A . Sin, L . F brega, M . T . D . O rlando, A . G . Cunha, S . Piol, E . Baggio-Saitovitch and X . Obradors, *Physica C*, 328 (1999) 80.

[19] A . Sin, A . G . Cunha, A . Calleja, M . T . D . O rlando, F . G . E m m erich, E . Baggio-Saitovitch, M . Segarra, S . Pioland X . Obradors, *Adv. M att.* 10 (1998) 1126.

[20] O . Chmaissem , P . G uptasarma, U . W elp, D . G . H inks and J . D . Jorgensen, *Physica C* 292 (1997) 305.

[21] M . T . D . O rlando, E . V . L . de M ello, C . A . C . Passos, M . R . C . Caputo, L . G . M artinez, B . Zeini, E . S . Y que, W . Vanoni and E . Baggio-Saitovitch, *Physica C*, 364–365 (2001) 350.

[22] G . C . MacIntosh and A . B . Kaiser, *Physical Review B*, 54, (1996) 12569

[23] R . P . Gupta and M . G upta, 51 (1995) 11760.

[24] S . D . Oberelli, J . R . Cooper, and J . L . Tallon, *Physical Review B*, 46 (1992) 14928.

[25] C . K . Subram aniam , M . Parantham an and A . B . K aiser, Physical Review B 51 (1995) 1330.

[26] C . A . C . Passos, M . T . D . O rlando, A . A . R . Femandes, F . D . C . O liveira, D . S . L . Simonetti, J.F . Fardin H . Belich Jr and M . M . Ferreira Jr , Physica C 519 (2005) 25.

[27] Y . Ando, S . K om iya, K . Segawa, S . O no and Y . K urita, cond-mat/0403032.

[28] S . H . Naqib, J . R . Cooper, J . L . Tallon, R . S . Islam , and R . A . Chakalov, Phys. Rev. B 71 (2005) 054502.

[29] V . L . G inzburg, 1960 F iz. T verd. Tela, 2 2031 Sov. Phys. – Solid State, 2 (1960) 1824.

[30] L . G . A slam asov and A . I . Larkin, Sov. Phys. – Solid State 10 (1968) 875.

[31] W . E . Lawrence and S . D oniach, in Proceedings of the 12th International Conference on Low Temperature Physics, Kyoto, Japan, edit by E . K anda (Keigaku, Tokyo) (1971) 361.

[32] R . J . W ijngaarden, D . Tristán Jover and R . G riessen, Physica B 265 (1999) 128.

[33] A . J . Batista-Leyva, M . T . D . O rlando, L . R ivero, R . Cobas and E . A ltshuler, Physica C 383 (2003) 365.

[34] J . Roa-Rojas, P . Pureur, L . M endonça-Ferreira, M . T . D . O rlando and E . B aggio-Saitovitch, Supercond. Sci. Technol., 14 (2001) 898.

[35] S . H . Naqib, J . R . Cooper, J . L . Tallon and C . Panagopoulos, Physica C 387 (2003) 365.

## 6 List of Figure

Figure 1 - The temperature dependence of electrical resistivity of the (Hg,Re)-1223 sample for  $J = 1.5 \text{ A/cm}^2$ . The inset shows the  $T$  determine from fitting up to 200K using  $J = 0.7 \text{ A/cm}^2$ .

Figure 2 - XRD patterns showing the main precursor phases for different thermal treatments: (#) represents  $\text{BaCuO}_{2+x}$ , (\*) represents  $\text{Ba}_2\text{Cu}_3\text{O}_{5+x}$ , (413) represents  $\text{Ba}_4\text{CaCu}_3\text{O}_{8+x}$ , and (&) represents  $\text{Ca}_5\text{Re}_2\text{O}_{12}$ .

Figure 3 - XRD patterns of the precursor ceramics with different oxygen partial pressure. The identified phases were:  $\text{BaCuO}_{2+x}$ ,  $\text{Ba}_2\text{Cu}_3\text{O}_{5+x}$ ,  $\text{Ba}_4\text{CaCu}_3\text{O}_{8+x}$ ,  $\text{Ca}_5\text{Re}_2\text{O}_{12}$  and  $\text{Ca}_2\text{CuO}_3$ .

Figure 4 - XRD patterns of the  $\text{Hg}_{0.82}\text{Re}_{0.18}\text{Ba}_2\text{Ca}_2\text{Cu}_3\text{O}_{8+}$  polycrystalline samples with different partial pressure of oxygen. The symbol (1223) represents the (Hg,Re)-1223 phase.

Figure 5 - Thermopower of the (Hg,Re)-1223 samples produced with different oxygen partial pressure during the process of precursor annealing.

Figure 6 - SEM image performed on optimally doped sample (sample B).

Figure 7 - Isotherms of the average voltage as a function of applied current. For  $T = 140 \text{ K}$ , it was used linear and polynomial fit, while for  $T = 170 \text{ K}$  the adjustment was a linear regression for sample B.

Figure 8 - The first and second derivative of resistance with respect to the temperature for (a) sample A, (b) sample B and (c) sample C. It was applied  $J = 1 \text{ A/cm}^2$ .

Figure 9 - Fluctuation conductivity in logarithmic scale for the sample B. The linear fitting indicate 3D ( $\beta = -1/2$ ) and 2D ( $\beta = -1$ ) behaviors.

Figure 10 – The calculated values of  $T_c$  and  $T$  as function of the charge carrier density.

## 7 List of Tables

Table 1: The values of oxygen partial pressure, critical temperature, thermoelectric power signal at 290K and hole number per Cu-O layer.

sample	$P_{O_2}$ (bar)	$T_c$ (K)	$S$ (V/K)	$p$ (hole/Cu-O)
A	0.05	132.6	3.0	0.15
B	0.10	133.2	1.8	0.16
C	0.15	132.7	0.5	0.17

Table 2: Sample composition obtained by EDS measurements. The value  $\langle d \rangle$  is the average junction size of the grain carried out by a SEM image analysis [8].

sample	Grain center	Grain board	$\langle d \rangle$ (m)
A	$H_{0.83}Re_{0.17}Ba_{1.98}Ca_{2.01}Cu_{2.98}O_{8+}$	$H_{0.78}Re_{0.22}Ba_{1.98}Ca_{2.02}Cu_{3.01}O_{8+}$	2.1
B	$H_{0.80}Re_{0.20}Ba_{1.99}Ca_{2.00}Cu_{2.98}O_{8+}$	$H_{0.82}Re_{0.18}Ba_{2.02}Ca_{2.03}Cu_{2.99}O_{8+}$	2.7
C	$H_{0.79}Re_{0.21}Ba_{2.03}Ca_{1.98}Cu_{2.99}O_{8+}$	$H_{0.83}Re_{0.17}Ba_{2.01}Ca_{1.97}Cu_{3.01}O_{8+}$	2.4

Table 3: Some parameters of the fluctuation conductivity

sample	$T_c$ (K)	$T_{Scf}$ (K)	$(T_{Scf} - T_c) = T_c$	$T$ (K)	$U_c$ (meV)
A	132.6	148	1	0.116	160 2 4.96
B	133.2	141	1	0.0586	155 2 3.63
C	132.7	137	1	0.0324	151 2 2.83

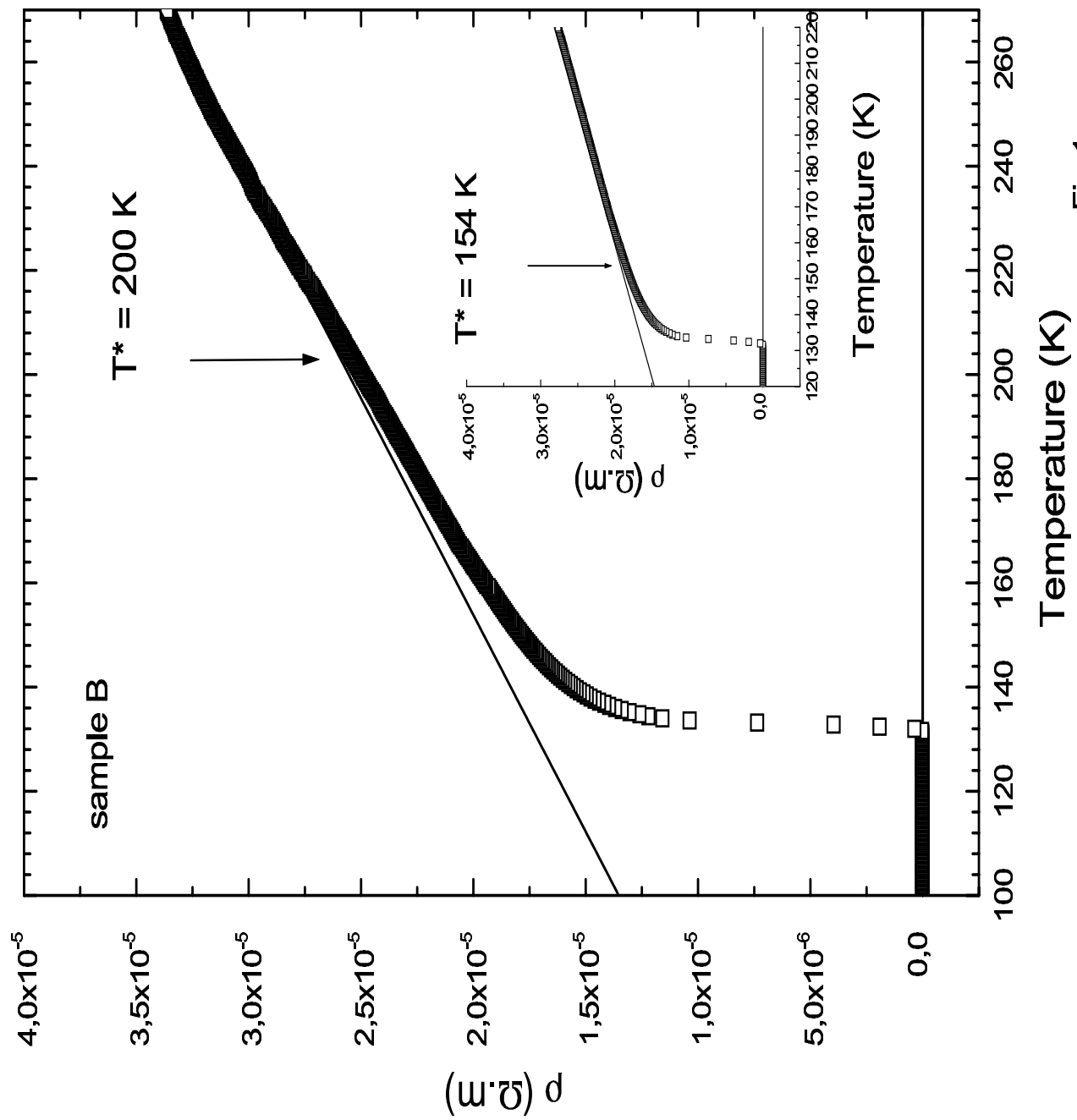
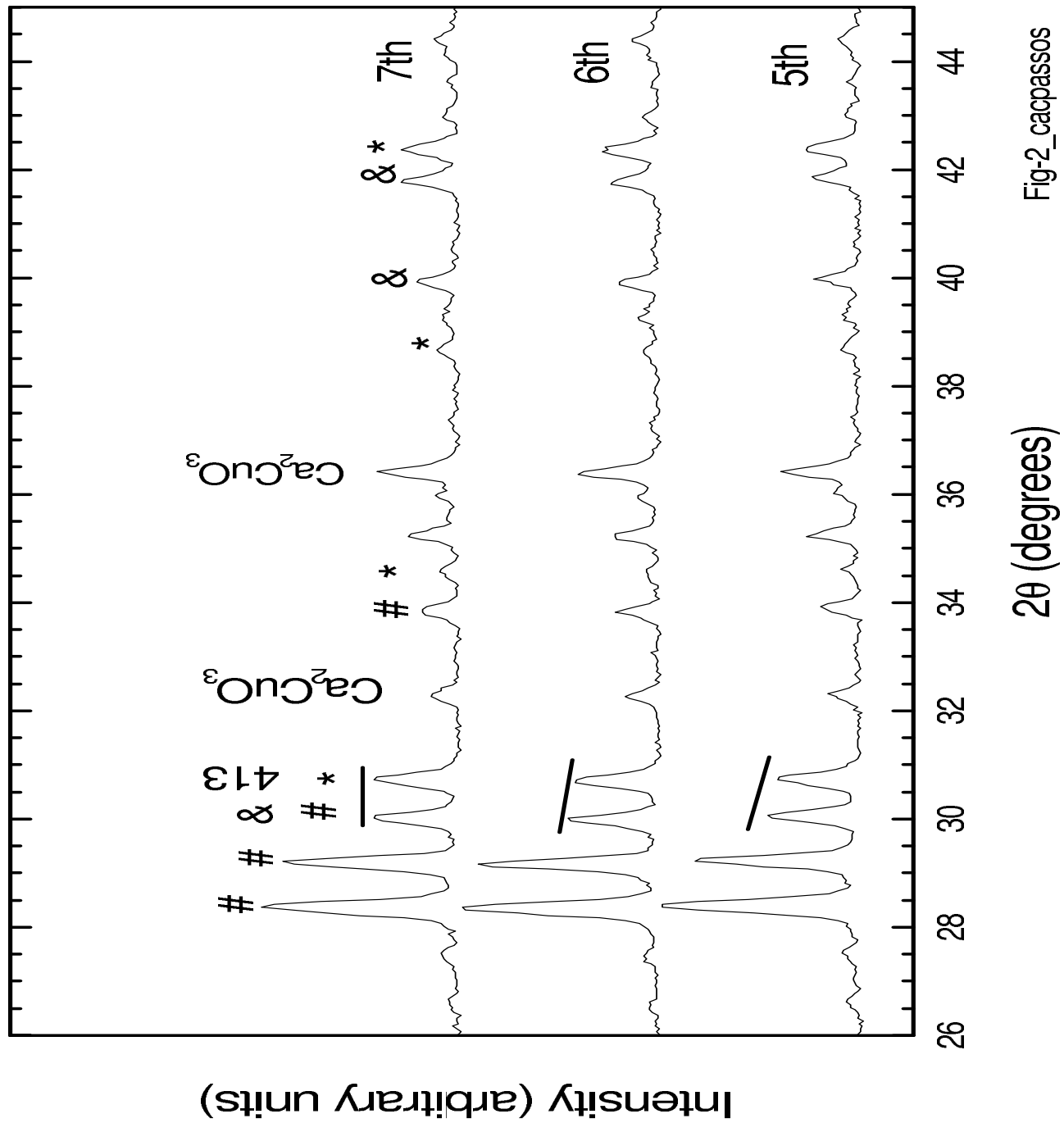


Fig-1\_cacpassos



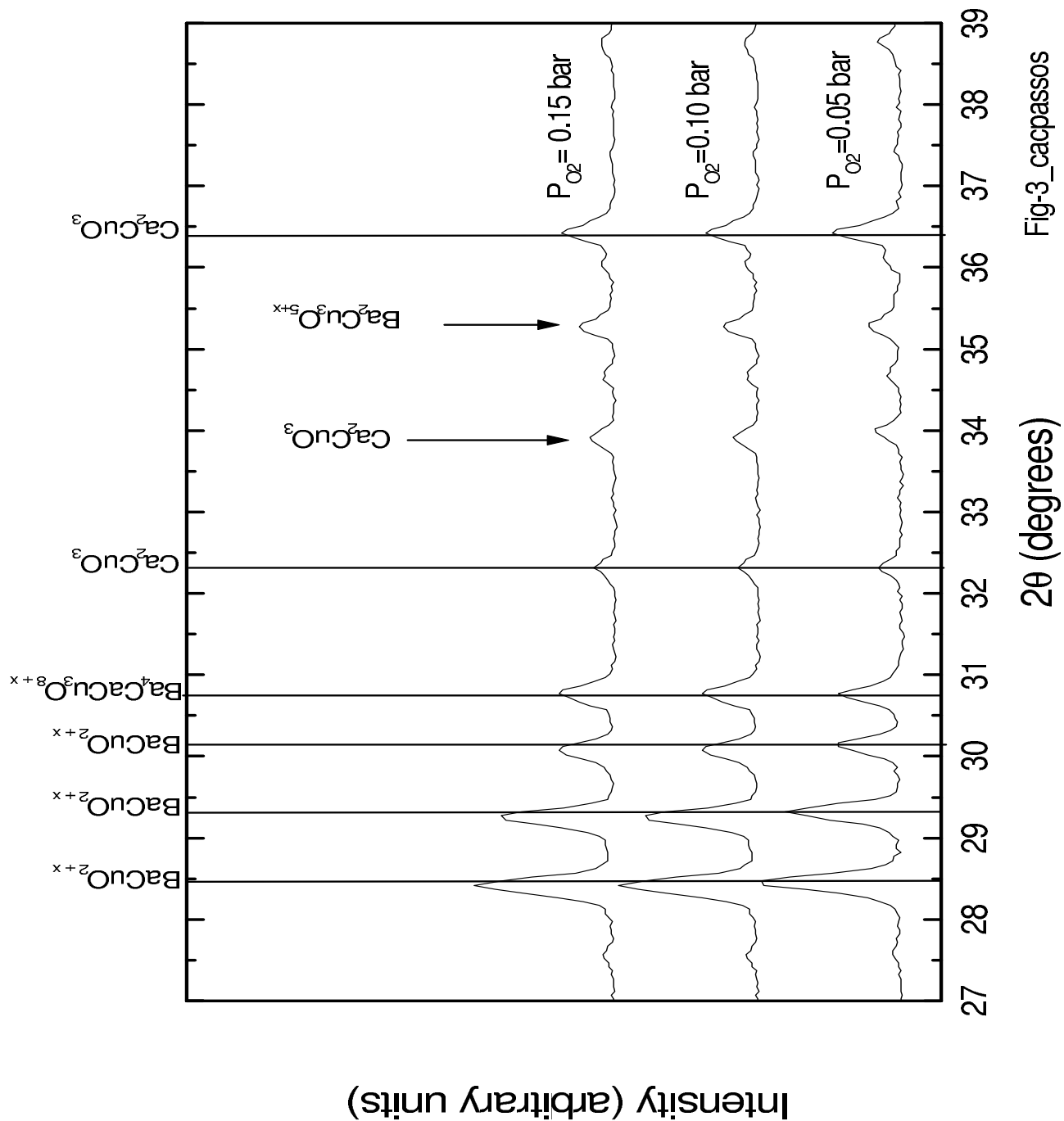
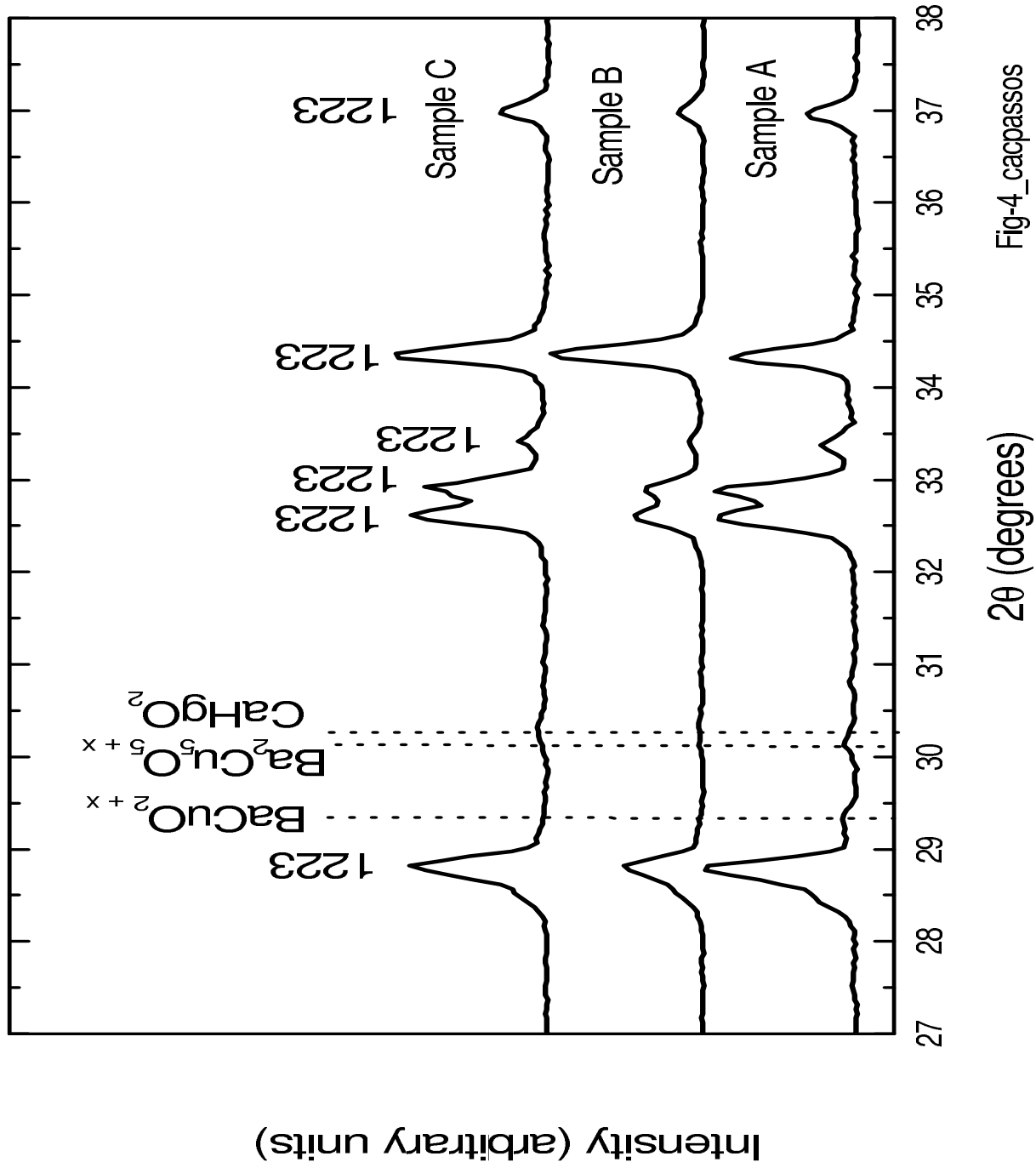
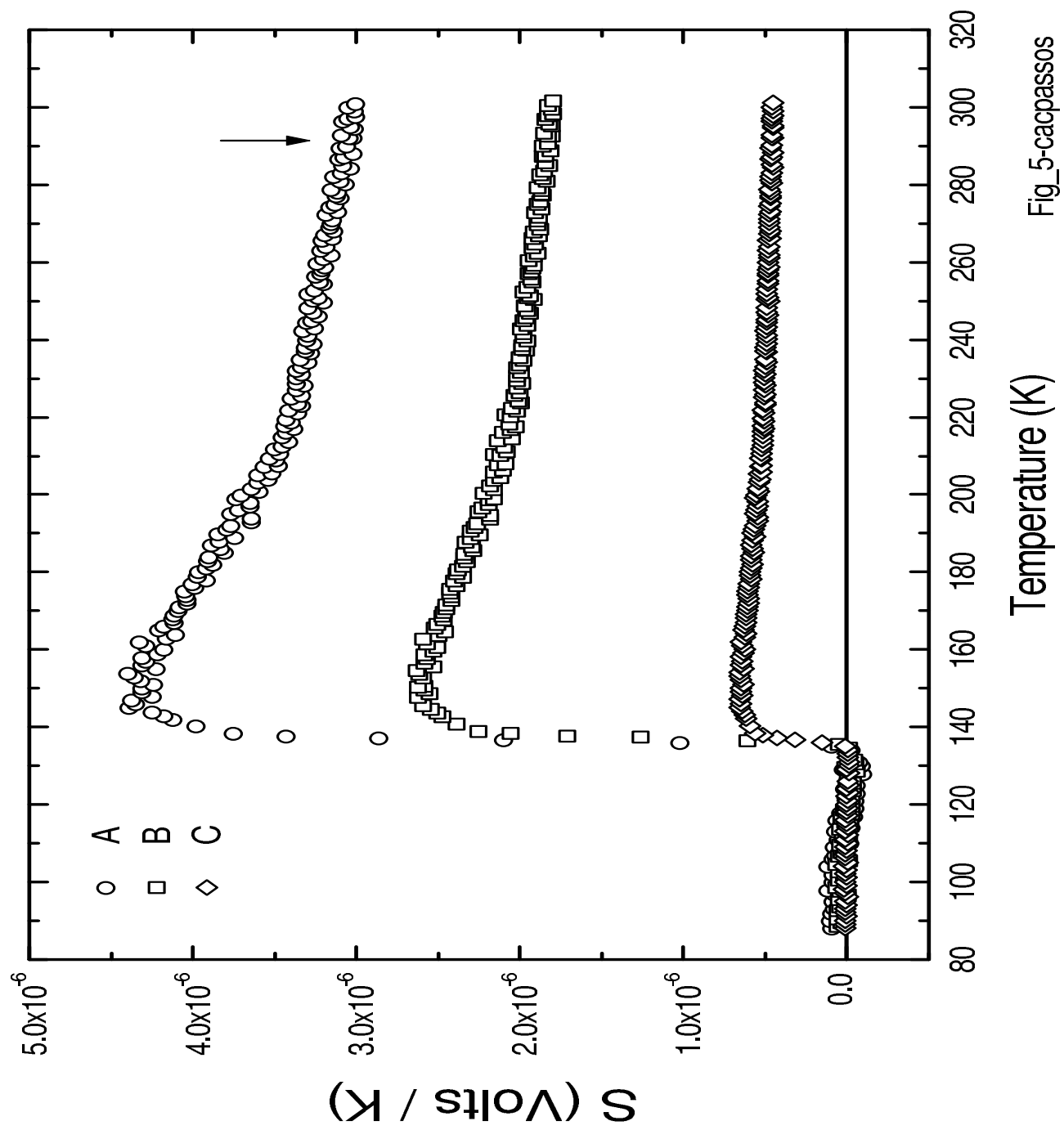


Fig-3\_cacpassos





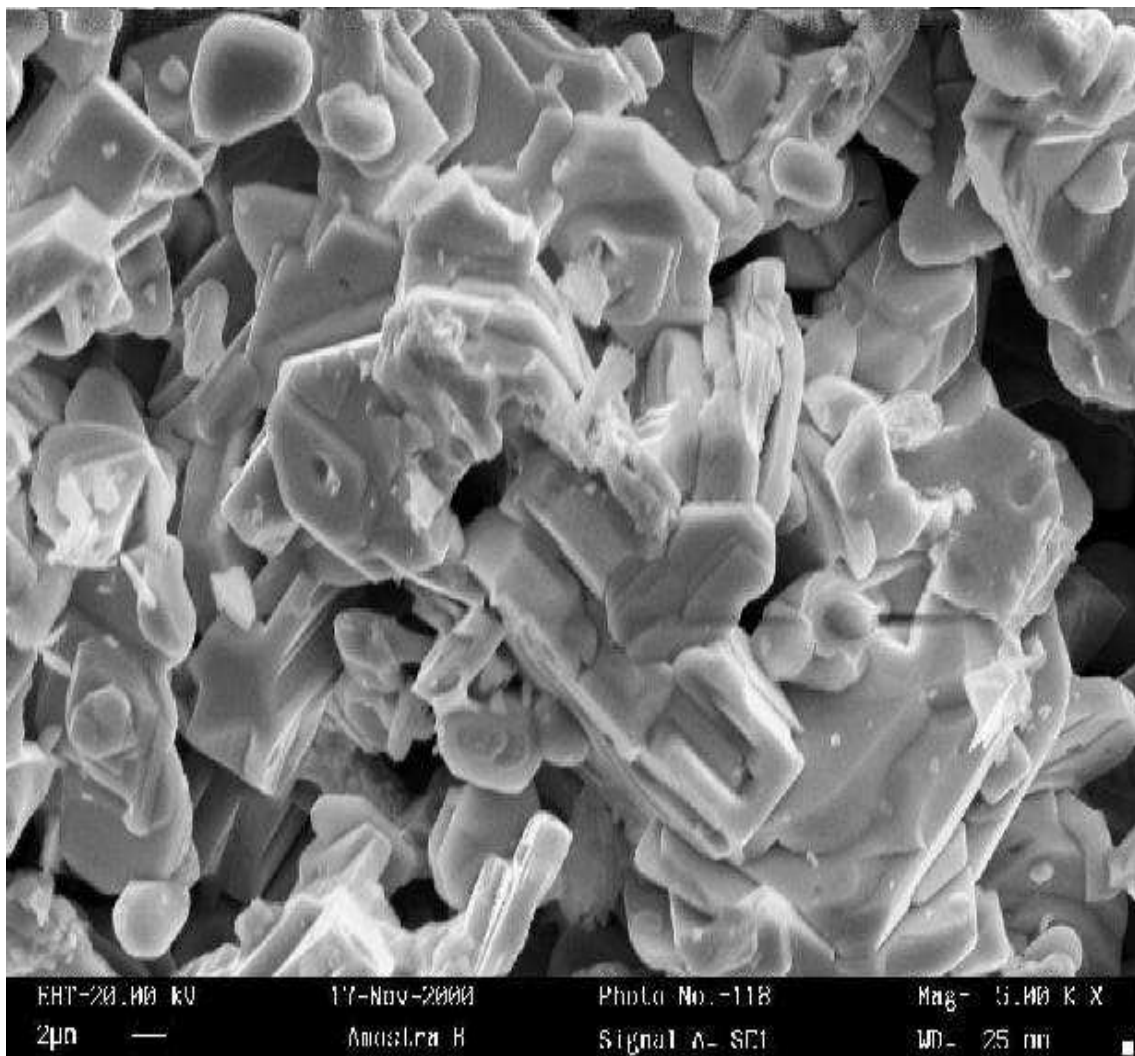
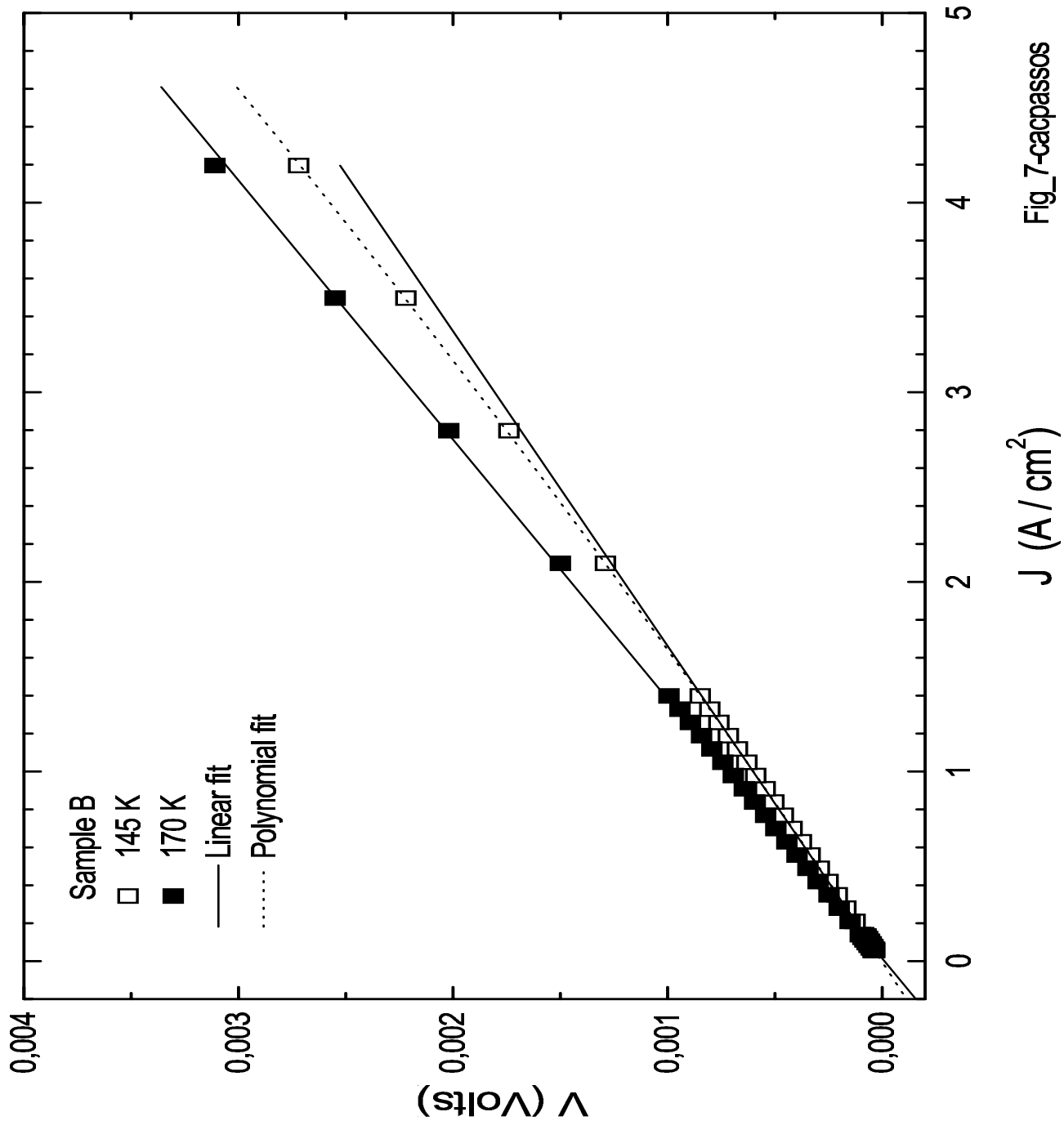
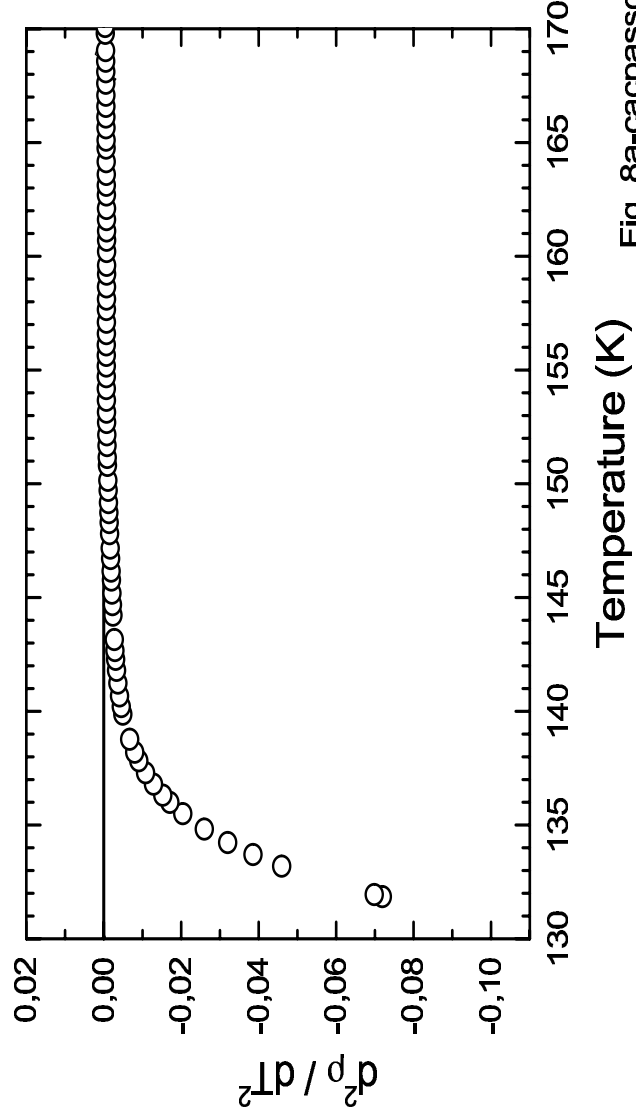
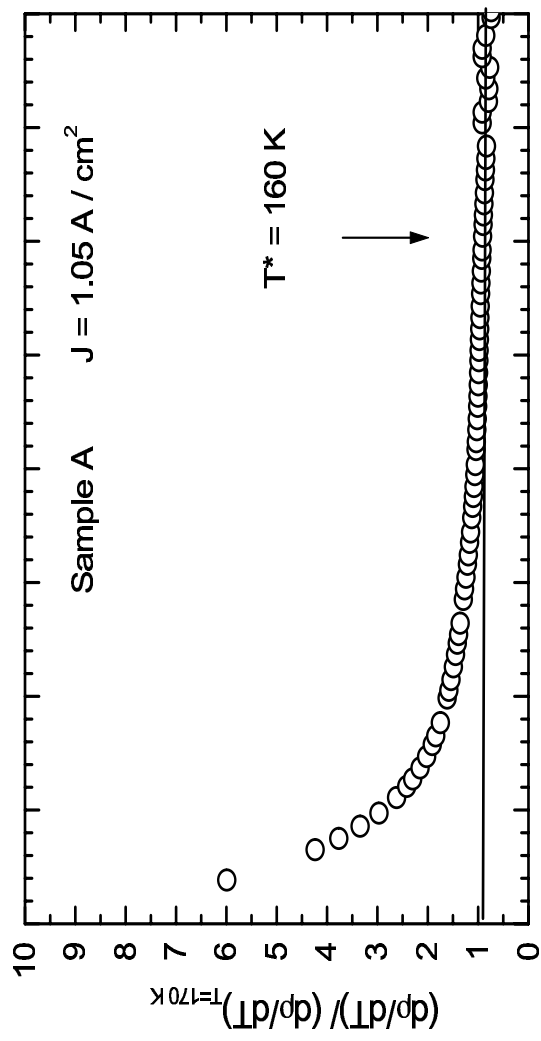
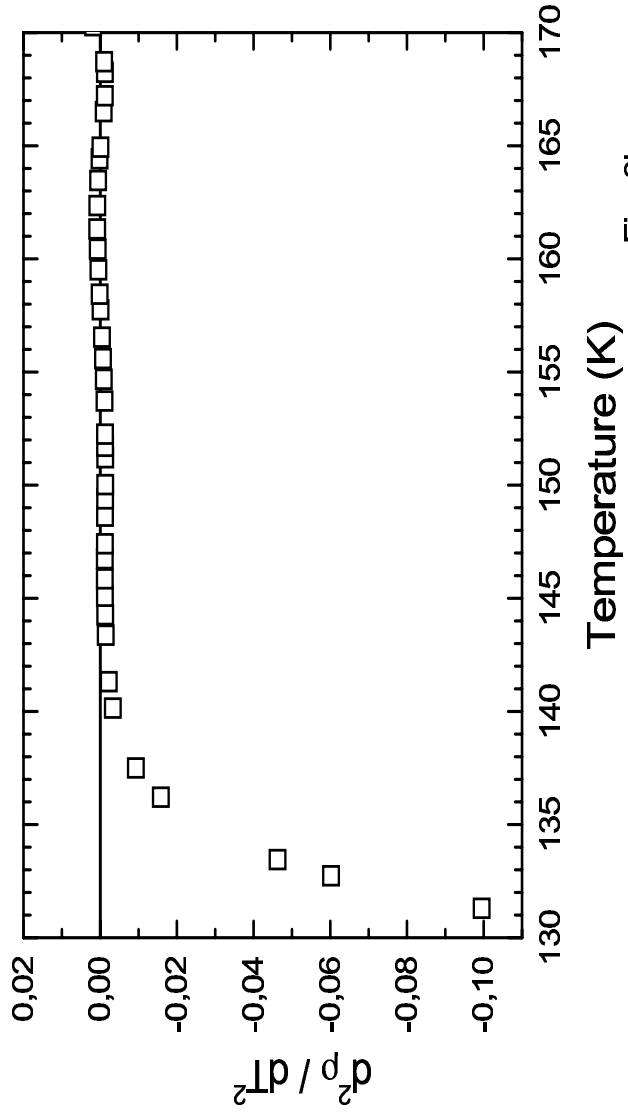
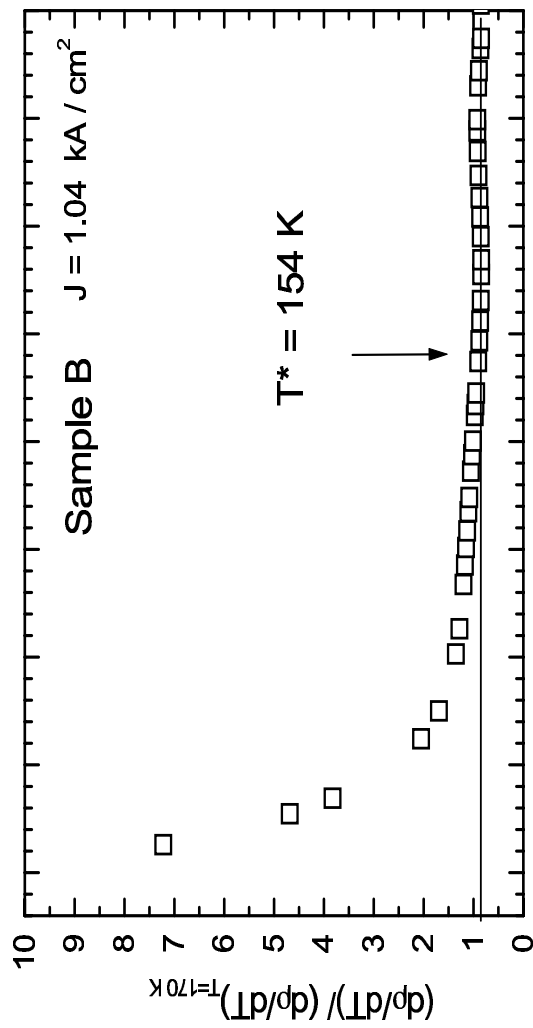


Fig-6-cacpassos





Fig\_8a-cacpassos



Fig\_8b-cacpassos

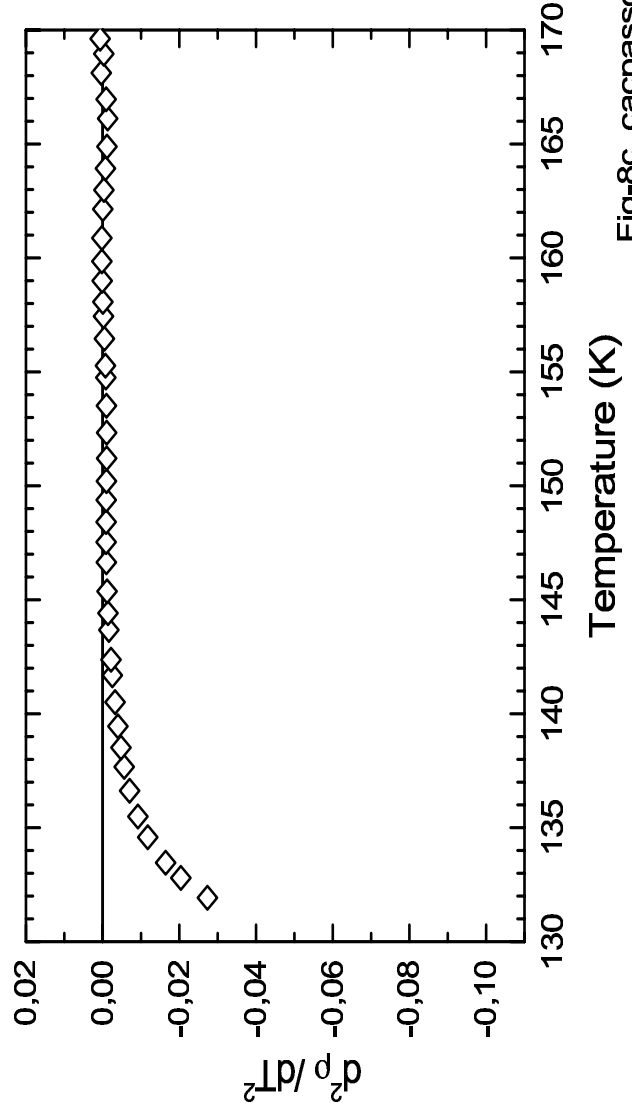
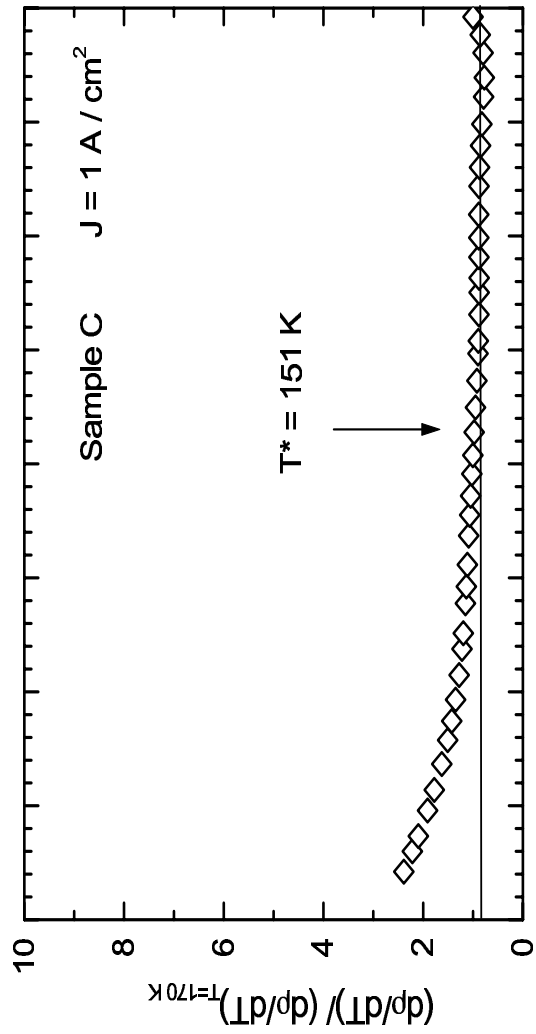
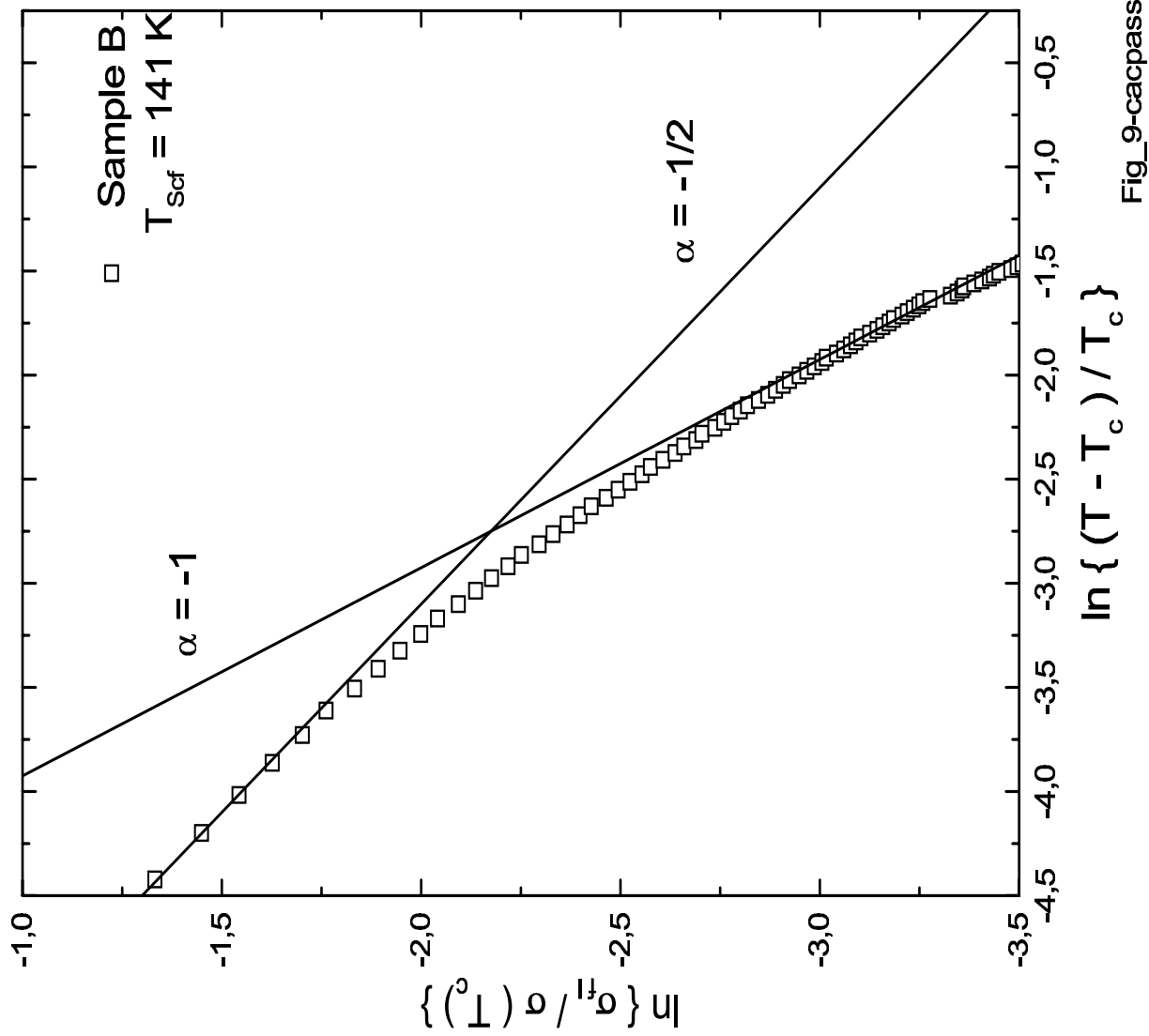


Fig-8c\_cacpassos



Fig\_9-cacpassos

